

Kinematic Analysis of the Double Wishbone Suspension System

Madhu Kodati

Department of Engineering Design
 Indian Institute of Technology Madras
 Chennai, India
 madhukodati@gmail.com

Sandipan Bandyopadhyay

Department of Engineering Design
 Indian Institute of Technology Madras
 Chennai, India
 sandipan@iitm.ac.in

Abstract—The double wishbone suspension is used commonly in high performance vehicles due to its superior kinematic response. However, its kinematics is very complicated, and to the best of the authors' knowledge, no reported analysis of the same for the full spatial model of the suspension exists in literature. This paper presents such a solution, building upon two key elements in the formulation and solution stages, respectively: the use of Rodrigue's parameters to develop an algebraic set of equations representing the kinematics of the mechanism, and the computation of Gröbner basis as a method of solving the resulting set of equations. It is found that the final univariate equation representing all the kinematic solutions for a given pair of steering and road profile inputs is of 64 degree – which explains the complexity observed in the kinematics of the mechanism. The real roots of this polynomial are extracted, and the solutions to the kinematic problem are computed for a particular set of inputs for the sake of illustration of the proposed formulation. The numerical accuracy of the solutions is verified by computing the residuals of the original set of kinematic constraints. The configurations of the mechanism for the real solutions are shown graphically.

Keywords: Double wishbone suspension, Spatial kinematics, Polynomial equations, Gröbner basis, Rodrigue's parameters

I. INTRODUCTION

The double wishbone is a popular suspension architecture for high performance cars. Kinematically, the suspension mechanism can be modelled as a combination of two spatial mechanisms: a four-bar, and a five-bar, which are coupled at the *king-pin* (see Fig. 1). The design involves a relatively large number of elements, and thus has a reasonably large design space. This affords better control over the kinematic response of the suspension. For instance, toe variation due to road inputs can be significantly reduced by the proper design of a double wishbone suspension [1]. For the same reason, however, the kinematics of the mechanism is significantly complicated. The mechanism possesses two degrees-of-freedom: one accounting for the steering input s , and the other accommodating the jounce and rebound, modelled as the *road profile* input y , as shown in Fig. 2. Finding the *output* or the *response* of the mechanism to these inputs, i.e., determining the location and orientation

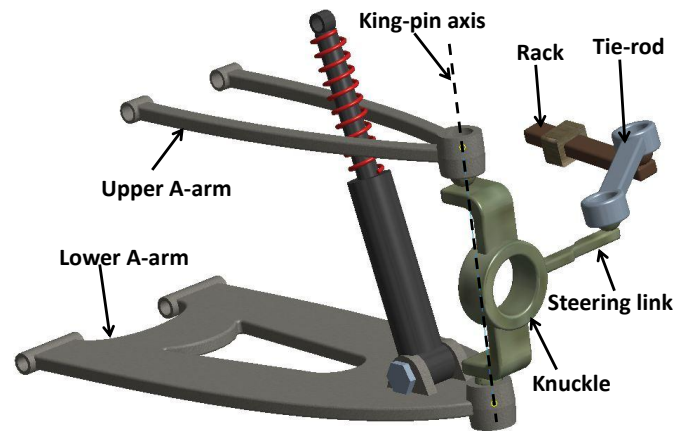


Fig. 1. Solid model of the double wishbone suspension

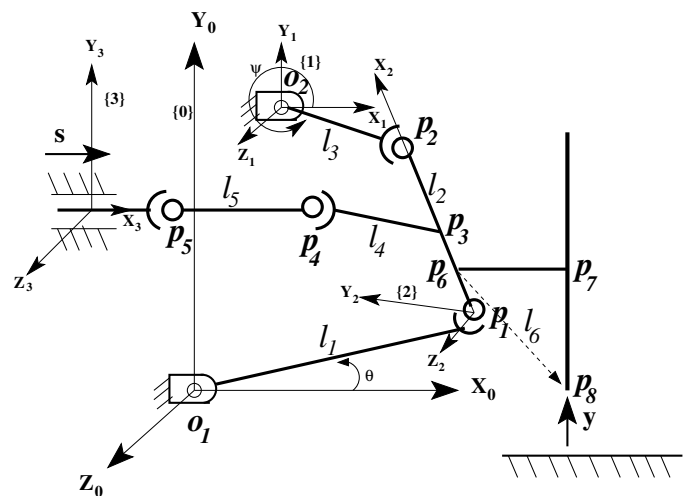


Fig. 2. Schematic of the double wishbone suspension mechanism

of the kingpin axis (KPA) for a combination of s, y , is a formidable task. To the best of the knowledge of the authors, this problem remains unsolved as yet. As an alternative to y , the lower A-arm angle, θ , has been used as a *surrogate input* to simplify the kinematic analysis [2]. In [3], one of the Euler angles representing the orientation of the KPA has been used for the same purpose.

In this paper, a method is presented to find the kinematic response of the double wishbone suspension (abbreviated as DWS henceforth) to a combination of road, and steering inputs. The kinematics of the mechanism is formulated in an *algebraic* manner, and the orientation of the KPA is represented in terms of the Rodrigue's parameters (e.g., [4]), $\mathbf{c} = (c_1, c_2, c_3)^T$. Such a formulation, aided by extensive symbolic computations, eventually leads to a set of three quartic equations in the three Rodrigue's parameters. Attempts to reduce the system of equations further while retaining all the parameters and variables in their generic symbolic form proves to be futile at this point. Thus, numeric values of all the parameters as well as the inputs s, y are used to render the equations amenable to further analysis. The Gröbner basis of the ideal generated by these equations is computed next, leading to a univariate polynomial of degree 64 in c_3 . This equation is solved numerically, and its real roots are processed further to completely determine the configuration of the DWS for a given set of inputs. The computational steps for one combination of inputs have been studied in this paper, and the numerical accuracy of the solutions have been ascertained by means of a study of the residuals of the original *loop-closure* equations.

The rest of the paper is organised as follows: in Section 2, the formulation of the kinematic constraints and their solution is presented in details, with the help of a numerical example. In Section 3, the paper is concluded.

II. KINEMATIC ANALYSIS OF DOUBLE WISHBONE SUSPENSION SYSTEM

The eventual success in solving any position kinematics problem relies upon appropriate kinematic modelling, compact formulation, as well as efficient solution techniques. The details of these, as applied to the present problem, are presented in this section. In order to simplify the kinematic model, standard assumptions, e.g., rigid links, ideal joints, exact knowledge of all the geometric parameters etc., are made. The following are assumed further:

- The chassis is considered the *fixed* or the *ground* link in the mechanism.
- The universal joint between the tie-rod and the rack is replaced by a spherical joint.

A. Geometry of the DWS

The schematic of the DWS mechanism is shown in the Fig. 2. Three coordinate systems are used to define the system. The global frame of reference $\{0\}$ is attached to ${}^0\mathbf{o}_1$

and its Z -axis (denoted by Z_0) is along the axis of the hinges of the lower A-arm. Link 1 moves in the X_0Y_0 plane. Two different *body-fixed* frame of references, namely $\{1\}$ and $\{2\}$, are attached to ${}^0\mathbf{o}_2$ and ${}^0\mathbf{p}_1$, respectively. The Z_1 -axis of $\{1\}$ is aligned to the axis of the hinges of the upper A-arm, and Link 3 is confined to the X_1Y_1 plane. The X_2 -axis of $\{2\}$ is along the link vector ${}^0\mathbf{l}_2 = {}^0\mathbf{p}_2 - {}^0\mathbf{p}_1$, and the plane X_2Y_2 contains the Link 4.

Any vector in the body-fixed frames of reference can be *transformed* to the global frame of reference by pre-multiplying with an appropriate rotation matrix $\mathbf{R} \in SO(3)$ (e.g., [5]). The rotation matrix ${}^1_0\mathbf{R}$ relates $\{1\}$ to $\{0\}$, which can be parameterised in terms of the X - Y - Z Euler angles, $(\alpha_1, \alpha_2, \alpha_3)$ (e.g., [5]):

$${}^1_0\mathbf{R} = \mathbf{R}_X(\alpha_1)\mathbf{R}_Y(\alpha_2)\mathbf{R}_Z(\alpha_3),$$

where, in general, $\mathbf{R}_X(\theta)$, $\mathbf{R}_Y(\theta)$, $\mathbf{R}_Z(\theta)$ represent CCW rotation through an angle θ , about the axes X , Y , and Z , respectively. The rotation matrix ${}^2_0\mathbf{R}$ relates $\{2\}$ to $\{0\}$ in the same manner. However, it is parameterised in terms of the Rodrigue's parameters, $\mathbf{c} = (c_1, c_2, c_3)^T \in \mathbb{R}^3$ (e.g., [4]). This is a key step in the kinematic modelling, as it leads to an *algebraic* description of the orientation of the KPA, which in turn, helps in formulating the *loop-closure* equations in algebraic terms, as explained in the next subsection.

B. Formulation of the loop-closure equations

The DWS is a combination of a spatial four bar loop, $\mathbf{o}_1\mathbf{p}_1\mathbf{p}_2\mathbf{o}_2\mathbf{o}_1$, and a spatial five bar loop, $\mathbf{o}_1\mathbf{p}_1\mathbf{p}_4\mathbf{p}_5$. The rack/steering input is given to the point ${}^0\mathbf{p}_5$, and the road profile input is applied to the point ${}^0\mathbf{p}_8$ (see Fig. 2). The end points of Link 2 can be expressed as:

$${}^0\mathbf{p}_1 = {}^0\mathbf{o}_1 + \mathbf{R}_{Z_0}(\theta)[l_1, 0, 0]^T, \text{ and} \quad (1)$$

$${}^0\mathbf{p}_2 = {}^0\mathbf{o}_2 + {}^1_0\mathbf{R}\mathbf{R}_{Z_1}(\psi)[l_3, 0, 0]^T, \quad (2)$$

respectively. The vector ${}^0\mathbf{l}_2$ can be expressed as:

$${}^0\mathbf{l}_2 = {}^0\mathbf{p}_2 - {}^0\mathbf{p}_1, \text{ or} \quad (3)$$

$${}^0\mathbf{l}_2 = {}^2_0\mathbf{R}[l_2, 0, 0]^T. \quad (4)$$

From (1-4), one can write:

$${}^0\mathbf{o}_2 - {}^0\mathbf{o}_1 + {}^1_0\mathbf{R}\mathbf{R}_{Z_1}(\psi)[l_3, 0, 0]^T - \mathbf{R}_{Z_0}(\theta)[l_1, 0, 0]^T - {}^2_0\mathbf{R}[l_2, 0, 0]^T = \mathbf{0}. \quad (5)$$

Equation (5) models the kinematics of the four-bar loop $\mathbf{o}_1\mathbf{p}_1\mathbf{p}_2\mathbf{o}_2\mathbf{o}_1$. The LHS of (5) is written compactly as:

$$\boldsymbol{\eta}_1 = (\eta_{1x}, \eta_{1y}, \eta_{1z})^T, \quad (6)$$

where η_{1x} , η_{1y} and η_{1z} are given by:

$$\eta_{1x} = -l_2(c_1^2 - c_2^2 - c_3^2 + 1) - c_\Delta l_1 \cos \theta + c_\Delta o_{2x} + c_\Delta l_3 \cos \alpha_2 (\cos \alpha_3 \cos \psi - \sin \alpha_3 \sin \psi), \quad (7)$$

$$\eta_{1y} = -2l_2(c_1 c_2 + c_3) + c_\Delta l_3 (\cos \psi (\sin \alpha_1 \sin \alpha_2 \cos \alpha_3 + \cos \alpha_1 \sin \alpha_3) + \sin \psi (\cos \alpha_1 \cos \alpha_3 - \sin \alpha_1 \sin \alpha_2 \sin \alpha_3)) - c_\Delta l_1 \sin \theta + c_\Delta o_{2y}, \quad (8)$$

$$\eta_{1z} = -2l_2(c_1c_3 - c_2) + c_\Delta l_3(\cos\psi(\sin\alpha_1 \sin\alpha_3 - \cos\alpha_1 \sin\alpha_2 \cos\alpha_3) + \sin\psi(\cos\alpha_1 \sin\alpha_2 \sin\alpha_3 + \sin\alpha_1 \cos\alpha_3)) + c_\Delta o_{2z}, \text{ and} \quad (9)$$

$c_\Delta = 1 + c_1^2 + c_2^2 + c_3^2$. The end points of Link 5 can be expressed as:

$${}^0\mathbf{p}_4 = {}^0\mathbf{p}_1 + {}^0_2\mathbf{R}[rl_2, 0, 0]^T + {}^0_2\mathbf{R}^2\mathbf{l}_4, \text{ and} \quad (10)$$

$${}^0\mathbf{p}_5 = [p_{5x} + s_x, p_{5y} + s_y, p_{5z} + s_z]^T, \quad (11)$$

where rl_2 is distance between ${}^0\mathbf{p}_1$ and ${}^0\mathbf{p}_3$; ${}^2\mathbf{l}_4 = (l_{4x}, l_{4y}, l_{4z})^T$ (expressed in $\{2\}$), and ${}^0\mathbf{s} = (s_x, s_y, s_z)^T$ is the rack input vector in $\{0\}$, given by:

$${}^0\mathbf{s} = {}^3_0\mathbf{R}[s, 0, 0]^T, \text{ where} \\ {}^3_0\mathbf{R} = \mathbf{R}_X(\beta_1)\mathbf{R}_Y(\beta_2)\mathbf{R}_Z(\beta_3),$$

i.e., $(\beta_1, \beta_2, \beta_3)$ are X-Y-Z Euler-angles relating $\{3\}$ to $\{0\}$. The vector ${}^0\mathbf{l}_5$ can be expressed as:

$${}^0\mathbf{l}_5 = {}^0\mathbf{p}_5 - {}^0\mathbf{p}_4.$$

The closure equations of the five bar loop $o_1\mathbf{p}_1\mathbf{p}_4\mathbf{p}_5o_1$ can be reduced to a single scalar equation:

$$({}^0\mathbf{p}_5 - {}^0\mathbf{p}_4) \cdot ({}^0\mathbf{p}_5 - {}^0\mathbf{p}_4) - l_5^2 = 0. \quad (12)$$

The expression on the LHS of (12) is denoted by η_2 . From the road input to the lower A-arm loop, $o_1\mathbf{p}_1\mathbf{p}_6\mathbf{p}_8$, one can write:

$$[p_{8x} + x, p_{8y} + y, p_{8z} + z]^T - {}^2_0\mathbf{R}^2\mathbf{l}_6 - {}^2_0\mathbf{R}[\rho l_2, 0, 0]^T - \mathbf{R}_{Z_0}(\theta)[l_1, 0, 0]^T - {}^0\mathbf{o}_1 = 0, \quad (13)$$

where x, z are the components of displacement of ${}^0\mathbf{p}_8$ in $\{0\}$ as a consequence of s and y departing from their initial values; ${}^2\mathbf{l}_6 = (l_{6x}, l_{6y}, l_{6z})^T = {}^2\mathbf{p}_8 - {}^2\mathbf{p}_6$. The parameter ρ is the fraction of distance between ${}^0\mathbf{p}_1$ and ${}^0\mathbf{p}_6$ of l_2 , given by: $\rho = \|{}^0\mathbf{p}_6 - {}^0\mathbf{p}_1\|/l_2$. The expression on the LHS of (13) is of the form:

$$\boldsymbol{\eta}_3 = (\eta_{3x}, \eta_{3y}, \eta_{3z})^T, \quad (14)$$

where η_{3x} , η_{3y} and η_{3z} are given by:

$$\eta_{3x} = -l_2\rho(c_1^2 - c_2^2 - c_3^2 + 1) - l_{6x}(c_1^2 - c_2^2 - c_3^2 + 1) - 2l_{6y}(c_1c_2 - c_3) - 2l_{6z}(c_1c_3 + c_2) + c_\Delta(-l_1 \cos\theta + p_{8x} + x), \quad (15)$$

$$\eta_{3y} = -2l_2\rho(c_1c_2 + c_3) - 2l_{6x}(c_1c_2 + c_3) - l_{6y}(-c_1^2 + c_2^2 - c_3^2 + 1) - 2l_{6z}(c_2c_3 - c_1) + c_\Delta(-l_1 \sin\theta + p_{8y} + y), \quad (16)$$

$$\eta_{3z} = -2l_2\rho(c_1c_3 - c_2) - 2l_{6x}(c_1c_3 - c_2) - 2l_{6y}(c_1 + c_2c_3) - l_{6z}(-c_1^2 - c_2^2 + c_3^2 + 1) + c_\Delta(p_{8z} + z). \quad (17)$$

The five equations, namely (7-9), (12), (16), define the kinematics of the DWS mechanism.

TABLE I. DETAILS OF THE LOOP-CLOSURE EQUATIONS OF THE DWS

Equation	LHS	Variables	Size (kb)
(7)	η_{1x}	$c_1, c_2, c_3, \cos\theta, \cos\psi, \sin\psi$	1.664
(8)	η_{1y}	$c_1, c_2, c_3, \cos\psi, \sin\theta, \sin\psi$	1.952
(9)	η_{1z}	$c_1, c_2, c_3, \cos\psi, \sin\psi$	1.888
(12)	η_2	$c_1, c_2, c_3, \cos\theta, \sin\theta$	78.232
(16)	η_{3y}	$c_1, c_2, c_3, \sin\theta$	2.944
(15)	η_{3x}	$c_1, c_2, c_3, x, \cos\theta$	3.280
(17)	η_{3z}	c_2, c_1, c_3, z	2.880

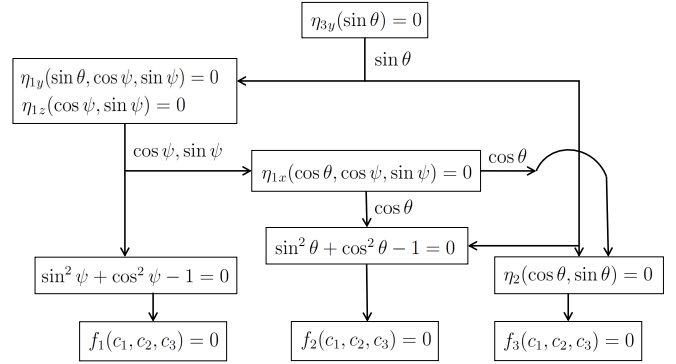


Fig. 3. Sequence of elimination of $\cos\theta, \sin\theta, \cos\psi$ and $\sin\psi$

C. Linear elimination of variables

The variables included and the *sizes*¹ of the equations obtained in the Section II-B are summarised in the Table I. The sequence of elimination of variables needs to be chosen so as to reduce the complexity of the resulting equations. To begin with, it is noted that all the seven equations are *linear* in terms of sines and cosines of the angles θ, ψ . Therefore, these trigonometric variables are eliminated first in a sequential manner, as shown schematically in Fig. 3. The details of the eliminations are presented below.

First, $\sin\theta$ is computed from (16), and substituted in (8). The functions η_{1y} and η_{1z} are linear in terms of $\sin\psi$ and $\cos\psi$. Hence (8), and (9), are solved linearly to obtain $\sin\psi$ and $\cos\psi$. The variable ψ is eliminated using the identity $\sin^2\psi + \cos^2\psi - 1 = 0$, which gives rise to the equation $f_1(c_1, c_2, c_3) = 0$. Note that f_1 is free of any other unknowns than those mentioned explicitly. Similarly, the expressions of $\sin\psi$ and $\cos\psi$ are substituted in (7), to obtain $\cos\theta$. Using the expressions of $\sin\theta$ and $\cos\theta$, the variable θ is eliminated using the identity $\sin^2\theta + \cos^2\theta - 1 = 0$, which leads to the equation $f_2(c_1, c_2, c_3) = 0$. Finally, The expressions of $\sin\theta$ and $\cos\theta$ are substituted in (12), to obtain the equation $f_3(c_1, c_2, c_3) = 0$.

The functions f_i are all quartic in c_i , and they are also

1. All the symbolic computations have been performed using the commercial computer algebra software, Mathematica. The “size”, in this context, refers to the amount of *computer memory* needed to represent/store an expression in Mathematica’s internal format.

TABLE II. GEOMETRIC PARAMETER VALUES OF THE DWS
(FROM [7], WITH MINOR MODIFICATIONS)

Parameter	Symbol	Value
Lower A-arm	l_1	0.420
Knuckle	l_2	0.162
Upper A-arm	l_3	0.260
Tie rod	l_5	0.519
Euler angles relating {1} to {0}	$(\alpha_1, \alpha_2, \alpha_3)$	$\left(\frac{-2\pi}{180}, \frac{-\pi}{180}, \frac{3\pi}{180}\right)$
Euler angles relating {3} to {0}	$(\beta_1, \beta_2, \beta_3)$	$\left(\frac{2\pi}{180}, \frac{\pi}{180}, \frac{-3\pi}{180}\right)$
Link 4 vector w.r.t. {2}	(l_{4x}, l_{4y}, l_{4z})	(0.0103,0)
Origin of {0}	${}^0\mathbf{o}_1$	(0,0,0)
Origin of {1}	${}^0\mathbf{o}_2$	(0.130,0.160,0)
Initial position of ${}^0\mathbf{p}_5$	(p_{5x}, p_{5y}, p_{5z})	(0.010,0.020,-0.400)
Initial position of ${}^0\mathbf{p}_8$	(p_{8x}, p_{8y}, p_{8z})	(0.480,-0.050,0)
${}^2\mathbf{l}_6$ w.r.t. {2}	(l_{6x}, l_{6y}, l_{6z})	(-0.209,0.007,-0.030)
$\ {}^0\mathbf{p}_1 - {}^0\mathbf{p}_3\ $ as a fraction of l_2	r	0.473
$\ {}^0\mathbf{p}_1 - {}^0\mathbf{p}_6\ $ as a fraction of l_2	ρ	0.312

symmetric in c_i . They may be written compactly as:

$$f_1(c_1, c_2, c_3) = \sum_{i=0}^4 \sum_{j=0}^4 \sum_{k=0}^4 u_{ijk} c_1^i c_2^j c_3^k, \quad (18)$$

$$f_2(c_1, c_2, c_3) = \sum_{i=0}^4 \sum_{j=0}^4 \sum_{k=0}^4 v_{ijk} c_1^i c_2^j c_3^k, \quad (19)$$

$$f_3(c_1, c_2, c_3) = \sum_{i=0}^4 \sum_{j=0}^4 \sum_{k=0}^4 w_{ijk} c_1^i c_2^j c_3^k; \quad (20)$$

where $i, j, k = 1, \dots, 4$, $i + j + k \leq 4$.

The coefficients u_{ijk} , v_{ijk} and w_{ijk} in (18-20) are functions of the geometric parameters of the DWS. These are obtained symbolically in Mathematica, and simplified using the *monomial-based canonical form* [6]. The sizes of the polynomials after simplification are 79.216 kb, 114.392 kb and 77.856 kb respectively.

D. Solution of the three quartic equations

It would be ideal indeed to solve (18-20) for the most general case, i.e., keeping all of their coefficients in symbolic form. However, attempts to eliminate two of the three remaining variables to obtain a *univariate* in the third variable in terms of symbolic coefficients did not succeed. Hence these equations are solved only for given numerical instances of design parameters (given in Table II), and inputs (s, y) . The solution procedure used, however, is *semi-analytical* in nature, and involves the computation of the *Gröbner basis* (e.g., [8]) generated by the *ideal* $\mathcal{F} = \langle f_1, f_2, f_3 \rangle$. This prevents the *degree-explosion*, which happens otherwise, if pair-wise resultants are computed. The details of this final stage of elimination and solution are presented in the rest of this section. The inputs used are $s = 0.1m$, $y = 0.05m$ for all the numerical computations.

1) *Numerical forms of (18-20)*: After the substitution of the numerical values as mentioned above, (18) becomes:

$$f_{1n} = 0.049c_1^4 - 0.980c_2c_1^3 - 11.369c_3c_1^3 + 0.093c_1^3 +$$

$$2.183c_2^2c_1^2 + 347.686c_3^2c_1^2 + 10.979c_2c_1^2 + 47.804c_2c_3c_1^2 - 5.515c_3c_1^2 + 0.139c_1^2 - 1.076c_2^3c_1 - 11.369c_3^3c_1 - 47.795c_2^2c_1 + 3.556c_2c_3^2c_1 + 47.989c_3^3c_1 + 3.460c_2c_1 - 12.093c_2^2c_3c_1 - 691.088c_2c_3c_1 - 12.875c_3c_1 + 0.102c_1 + 0.073c_2^4 + 0.049c_3^4 + 12.484c_2^3 - 0.093c_2c_3^3 - 0.980c_3^3 + 347.734c_2^2 + 0.139c_2^2c_3^2 + 11.760c_2c_3^2 + 2.183c_3^2 + 12.484c_2 - 0.102c_2^2c_3 - 5.611c_2^2c_3 - 47.998c_2c_3 - 1.076c_3 + 0.073. \quad (21)$$

The numerical coefficients are next converted to their *rational* forms in an approximate manner, up to a tolerance of $\epsilon = 10^{-10}$. This renders them better suited for the symbolic manipulations needed in the computation of the Gröbner basis. For instance, the expression for f_{1n} becomes:

$$f_{1r} = \frac{4721c_1^4}{97017} - \frac{132775c_2c_1^3}{135544} - \frac{1096375c_3c_1^3}{96433} + \frac{10299c_1^3}{111025} + \frac{793562c_2^2c_1^2}{363439} + \frac{30167705c_3^2c_1^2}{86767} + \frac{12880845c_2c_3c_1^2}{269453} - \frac{319509c_3c_1^2}{57932} + \frac{10558c_1^2}{76165} - \frac{68680c_2^3c_1}{63853} - \frac{1096375c_3^3c_1}{96433} - \frac{5198665c_2^2c_1}{108771} + \frac{419065c_2c_3^2c_1}{117844} + \frac{5112722c_2^2c_3c_1}{313424c_2c_1} - \frac{1316081c_2^2c_3c_1}{1316081} - \frac{106539}{90583} + \frac{108830}{108830} + \frac{51441166c_2c_3c_1}{74435} + \frac{16468c_1}{161679} + \frac{9305c_2^4}{128217} + \frac{4721c_3^4}{97017} + \frac{1274857c_2^3}{102121} - \frac{10299c_2c_3^3}{111025} - \frac{132775c_3^3}{135544} + \frac{102121}{32579566c_2^2} + \frac{10558c_2^2c_3^2}{10558c_2^2c_3^2} + \frac{1090489c_2c_3^2}{1090489c_2c_3^2} + \frac{93691}{793562c_3^2} + \frac{76165}{1274857c_2} + \frac{92728}{16468c_2^3c_3} - \frac{363439}{815519c_2^2c_3} + \frac{102121}{5954237c_2c_3} - \frac{161679}{68680c_3} + \frac{145336}{9305} - \frac{124051}{761467c_3c_1} - \frac{63853}{1677065c_2c_1^2} + \frac{128217}{59145} + \frac{152759}{152759}. \quad (22)$$

The functions f_2 and f_3 are treated similarly to obtain the corresponding expressions f_{2r} and f_{3r} with rational coefficients.

2) *Computation of the Gröbner basis and final solution*: The Gröbner basis of $\langle f_{1r}, f_{2r}, f_{3r} \rangle$ with the *lexicographical* order $c_1 \succ c_2 \succ c_3$ consists of three polynomials: $g_1(c_3)$, $g_2(c_2, c_3)$, and $g_3(c_1, c_3)$, respectively. Among these, g_1 is a univariate polynomial in c_3 of degree 64:

$$g_1 = a_0c_3^{64} + a_1c_3^{63} + \dots + a_{64} = 0. \quad (23)$$

Each of a_i are long integers; for instance, a_0 has 5924 digits. The polynomials g_2, g_3 are *linear* in c_2 and c_1 , respectively. Expressions for c_2 and c_1 can be obtained as:

$$c_2 = m_2/n_2, \quad (24)$$

TABLE III. VALUES OF θ , ψ , x AND z AND RESIDUALS OF (5), (12) AND (13) FOR $s = 0.1m$, $y = 0.05m$

c_1	c_2	c_3	θ	ψ	x	z	Residuals $\times 10^{-11}$		
							$\ \eta_1\ $	$ \eta_2 $	$\ \eta_3\ \times 10^{-6}$
-2.488	-3.312	1.358	0.351	0.519	-0.015	0.018	1.936	3.324	1.430
0.259	0.369	1.361	0.385	0.577	-0.064	-0.021	6.102	3.056	2.081
1.503	-13.694	-4.705	-0.0606	-1.093	0.097	0.018	1.661	1.271	1.734
-0.183	-0.621	-8.162	-0.0611	-1.093	0.093	-0.039	19.741	4.834	5.594

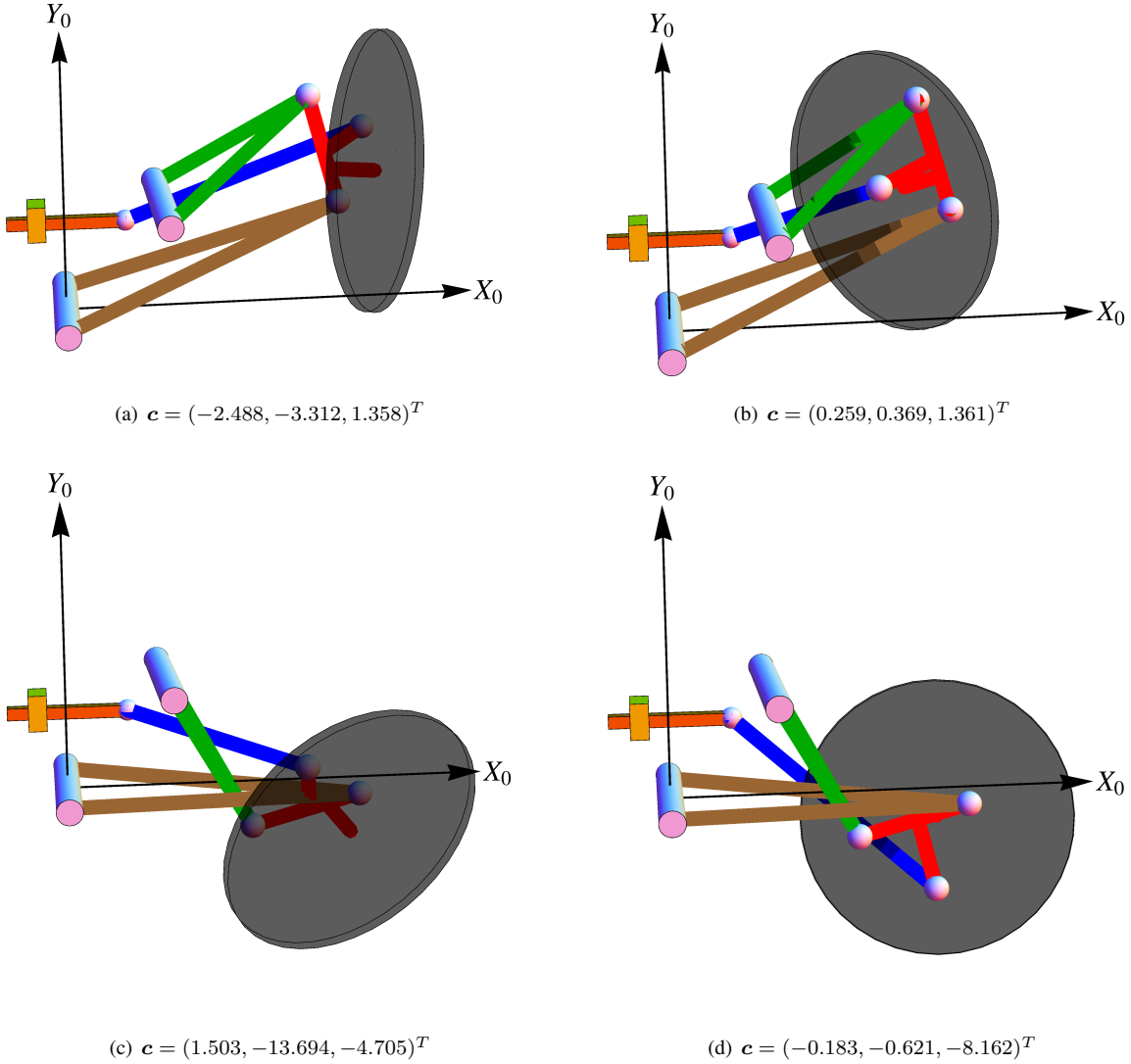


Fig. 4. Configurations corresponding to the real solutions of (18-20) for $s = 0.1m$, $y = 0.05m$

$$c_1 = m_1/n_1, \quad (25)$$

where m_1 , m_2 are polynomials in c_3 of degree 63 and n_1 , n_2 are integers. The extraction of the real roots of (23) using the Mathematica routine `NSolve`² yields $c_3 = 1.358, 1.361, -4.705, -8.162$. These solutions for c_3 are substituted back in (24-25) to obtain the corresponding

solutions for c_2 and c_1 :

$$c_2 = -3.312, 0.369, -13.694, -0.621;$$

$$c_1 = -2.488, 0.259, 1.503, -0.183.$$

The solutions of c_1 , c_2 and c_3 obtained from (23-25) are back-substituted in (7-9) and (15-17) to compute the

2. In order to obtain accurate solutions with `NSolve`, the “WorkingPrecision” parameter is needed to be set to a high value of 200 in this case.

corresponding solutions for θ , ψ , x and z . Numerical values of these variables are listed in the Table III. The residuals of the original loop-closure equations are also listed in the Table III, demonstrating the numerical accuracy of the solutions obtained. The configurations of mechanism for the real solutions of c_1 , c_2 and c_3 are shown in Fig. 4. As can be seen there, only one of the solutions, namely, the one depicted in Fig. 4(a), is realisable from a physical standpoint.

It may be noted here that the actual number of real solutions to this problem for a generic input is not known at this point. The univariate equation in c_3 is of degree 64, and it is possible that it has some roots at infinity at all configurations, leading to a lower limit for the number of possible real solutions. It may also be possible to factor the equation, leading to the identification of different assembly modes. However, all of these require much deeper study of the set of equations derived in this work, and it is too early to make any objective remark in this regard.

III. CONCLUSIONS

This paper presents a complete study of the position kinematics of the double wishbone suspension mechanism. Such a kinematic solution scheme is essential for detailed analysis or design of the suspension mechanism. The kinematic formulation used in this paper utilises an algebraic parametrisation of the orientation of the KPA. Using a simple scheme of elimination, the original set of five simultaneous algebraic-trigonometric equations, which define the kinematic constraints, are reduced to a set of three quartic equations. The solution of this reduced set of polynomial equations is done by computing the Gröbner basis of the ideal formed by the polynomials, which includes a univariate polynomial of degree 64. The numerical solutions obtained are verified by computing the residuals of the original set of equations at the solution point. Configurations of the DWS for all the real solutions obtained at a given set of inputs are shown graphically.

The main contribution of the paper is the solution of the position analysis problem of the DWS in its full complexity,

perhaps for the first time in reported literature. The key motivation behind this has been to develop a *kinematics back-end*, to support detailed analysis/optimisation of the DWS design, as well the study of its dynamics. While the present work attains the stated objective, it still relies upon very intensive, and specialised symbolic computations³, e.g., Gröbner basis computations and solutions of polynomial equations of high degree. In the future, it would be attempted to obtain the same solutions in the general case, purely by means of standard numerical computations.

REFERENCES

- [1] H. S. Jörnßen Reimpell and J. W. Betzler, *The Automotive Chassis: Engineering Principles*. SAE International, Warrendale, PA, 2001.
- [2] A. Arikere, G. Saravana Kumar, and S. Bandyopadhyay, "Optimisation of double wishbone suspension system using multi-objective genetic algorithm," in *Simulated Evolution and Learning*, vol. 6457 of *Lecture Notes in Computer Science*, pp. 445–454, Springer Berlin Heidelberg, 2010.
- [3] T. Uchida and J. McPhee, "Driving simulator with double-wishbone suspension using efficient block-triangularized kinematic equations," *Multibody System Dynamics*, vol. 28, no. 4, pp. 331–347, 2012.
- [4] J. M. Selig, *Geometric fundamentals of robotics*. New York: Springer, second ed., 1996.
- [5] A. Ghosal, *Robotics: Fundamental Concepts and Analysis*. New Delhi: Oxford University Press, 2009.
- [6] S. Bandyopadhyay and A. Ghosal, "Geometric characterization and parametric representation of the singularity manifold of a 6-6 Stewart platform manipulator," *Mechanism and Machine Theory*, vol. 41, pp. 1377–1400, Nov. 2006.
- [7] H. A. Attia, "Dynamic modelling of the double wishbone motor-vehicle suspension system," *European Journal of Mechanics A/Solids*, vol. 21, pp. 167–174, 2002.
- [8] D. Cox, J. Little, and D. O'Shea, *Ideals, Varieties, and Algorithms: An Introduction to Computational Algebraic Geometry and Commutative Algebra*. New York: Springer-Verlag, 1991.

3. It takes about 5 minutes to compute the real configurations corresponding to a particular set of inputs, using one core of an Intel(R) Core(TM) i7-3770 CPU running at 3.40 GHz, with 32 GB of RAM.